ATOMISTIC SIMULATIONS OF INTRINSIC AND EXTRINSIC POINT DEFECTS IN URANIUM

A Thesis
Presented to
The Academic Faculty

by

Benjamin Warren Beeler

In Partial Fulfillment
of the Requirements for the Degree
Masters of Science in the
School of Mechanical Engineering

Georgia Institute of Technology
December 2011

ATOMISTIC SIMULATIONS OF INTRINSIC AND EXTRINSIC POINT DEFECTS IN URANIUM

Approved by:

Dr. Chaitanya Deo, Advisor
School of Mechanical Engineering
Georgia Institute of Technology

Dr. Bojan Petrovic
School of Mechanical Engineering
Georgia Institute of Technology

Dr. Ting Zhu
School of Mechanical Engineering
Georgia Institute of Technology

Date Approved: 10/26/2011

ACKNOWLEDGEMENTS

Thank you to my family and friends for their continued support.

TABLE OF CONTENTS

LIST OF TABLES

LIST OF FIGURES

SUMMARY

Uranium (U) exhibits a high temperature body-centered cubic (b.c.c.) allotrope that is often stabilized by alloying with transition metals such as Zr, Mo, and Nb for technological applications. One such application involves U–Zr as nuclear fuel, where radiation damage and diffusion (processes heavily dependent on point defects) are of vital importance. Metallic nuclear fuels swell under fission conditions, creating fission product gases such as helium, xenon and krypton. Several systems of U are examined within a density functional theory framework utilizing projector augmented wave pseudopotentials. Two separate generalized gradient approximations of the exchange-correlation are used to calculate defect properties and are compared. The bulk modulus, the lattice constant, and the Birch–Murnaghan equation of state for the defect free b.c.c. uranium allotrope are calculated. Defect parameters calculated include energies of formation of vacancies in the α and γ allotropes, as well as self-interstitials, Zr, He, Xe and Kr interstitial and substitutional defects. The results for vacancies agree very well with experimental and previous computational studies. The most probable self-interstitial site in γ-U is the <110> dumbbell and the most probable defect location for dilute Zr in γ-U is the substitutional site. The most likely position for Xe and Kr atoms in uranium is the substitutional site. Helium atoms are likely to be found in a wide variety of defect positions due to the comparable formation energies of all defect configurations analyzed.

CHAPTER 1

INTRODUCTION

Metal alloy fuels have a long history in fast-reactor applications dating back to the earliest days of reactor development at the Metallurgical Laboratory of the University of Chicago [1,2,3]. Metallic fuel cores were employed in the sodium-potassium eutectic-cooled Experimental Breeder Reactor I (EBR-I), the world's first experimental fast neutron breeder reactor between 1951 and 1963. Its successor, the sodium-cooled Experimental Breeder Reactor II (EBR-II), was also powered by a number of metallic fuel cores during its operation from 1964 until 1992. The EBR-II was used to study the performance of a variety of experimental metal alloy fuels in addition to a myriad of other fuel types, including oxides and nitrides. Other fast reactors that have utilized metallic fuel cores include the Fermi reactor in the United States and the Dounreay reactor in the United Kingdom.

Metal alloy fuels have demonstrated superior performance in that they behave in a benign manner during core off-normal events, maintain integrity to high burnup, and lend themselves to low-loss recycling processes as well as ease of operation and low minor actinide (MA) fabrication loss under remote-handling conditions [4]. However, most of the fundamental properties and behavior of these materials have not been measured and are not well understood.

Some of the metallic fuel types used or tested in fast spectrum reactors were high-enriched uranium (HEU), Pu-Al alloys, U-Mo alloys, U-Pu-Zr alloys, and U-fissium and U-Pu-fissium alloys (fissium is a mixture of Zr, Nb, Mo, Ru, Rh, and Pd). In addition, many small thermal spectrum research and test reactors employ metallic fuel such as U-

Mo alloys in Al cladding or dispersion fuel of U-Mo alloy in Al matrix. Recent efforts to develop metal alloy fuels for actinide transmutation in either fast-flux reactors or accelerator-driven systems of a closed nuclear fuel cycle have included studies on U-Pu-MA-Zr and Pu-MA-Zr (MA = minor actinides = Np, Am, Cm) alloys. Most of these contain uranium as the base element with varying alloying additions. The alloying additions attempt to stabilize the high temperature body-centered cubic (b.c.c. gamma) phase at the expense of the anisotropic face-centered orthorhombic (alpha) phase. However, spent metallic fuels usually take the orthorhombic form.

Uranium, an actinide exhibiting delocalized f-electrons, exists in three solid allotropes: α (face-centered orthorhombic), β (body-centered tetragonal) and γ (body-centered cubic) [5]. At elevated temperatures, uranium transforms from α to β at approximately 935 K and β transforms to γ at approximately 1045 K [6].

One issue encountered with metallic U alloy fuels is swelling. The dramatic swelling of metallic fuels under irradiation is largely due to the incorporation of fission product gases in the fuel matrix during burnup. The specific isotopic yields for fission products (FP) vary based on fuel composition and the type of reactor. Three common gases present in the fission environment are helium, xenon and krypton. Research efforts [7] in the past have focused on understanding and predicting the constituent redistribution in metallic alloy fuels as this is of importance to the overall interpretation of fuel element behavior. However, unlike UO_2 commercial fuels, reliable experimental data on defect energies that impact fuel performance during its operation and subsequent long term storage are very scarce.

Several examinations of U via a first principles methodology have been performed on the orthorhombic and body-centered cubic structures of U. Soderlind [8] implemented a full-potential linear muffin-tin orbital (FPLMTO) method to calculate lattice and elastic constants of α-U. Lattice constants were predicted within 1% of experimental values [9], while the bulk modulus was slightly overestimated when compared to experiment [6]. Crocombette et al. [10] utilized a norm-conserving pseudopotential method with a very high cutoff energy (2448 eV), resulting in a greater variance of lattice parameters and a greater overestimation of the bulk modulus. Taylor [11] used a projector-augmented wave (PAW) pseudopotential developed for U by Kresse and Fürthmuller [12] with a cutoff energy of 253 eV to calculate the lattice constants of α-U and γ-U along with the bulk modulus of both allotropes. Taylor [11] also calculated the vacancy formation energy in the α allotrope. The lattice and elastic constants are predicted with comparable accuracy to the full-potential methods in the α allotrope, but the bulk modulus of the γ allotrope is highly overestimated when compared with experiment [5]. An analysis of bulk properties in the α and γ allotropes, as well as an analysis of defects in γ -U, was performed by Xiang et al. [13] utilizing a PAW pseudopotential. Lattice and elastic constants for α-U and γ-U correspond with experimental values [9, 5] and the vacancy formation energy is slightly underestimated with respect to vacancy formation energies estimated through positron annihilation spectroscopy [14]. Recently, PAW pseudopotential calculations have been performed analyzing defects in α-U [15].

From the preceding literature review, only two studies have attempted to calculate point defect properties in U; these have been calculations of the vacancy formation

energy in the α [11, 15] and the γ [13] allotropes. The explanation for such a limited scope of analysis on the defects lies partially in the inherent issues associated with a density functional theory (DFT) approach to the study of a high temperature allotrope and partially in computational limitations.

Density functional calculations are typically performed to calculate ground state properties, implying that the calculation is taking place at a temperature equal to 0 K. It has been shown, via the calculation of elastic constants, that the elastic shear constant ($C' = (C_{11} - C_{12})/2$) is negative in the body-centered cubic allotrope of U at 0 K [6]. Thus, at low temperatures, b.c.c. U is mechanically unstable. Computationally, this mechanical instability translates into an inability to calculate relaxed structures involving defects, due to the inherent localized deformation created by introducing a point defect. Several other systems, such as Zr, Ti, and Hf, also exhibit a high temperature body-centered cubic allotrope that is mechanically unstable at low temperature [16, 17].

Another issue relates to the size of the supercell studied. If a small supercell is analyzed, there can be cross-boundary effects due to the inherent periodicity of the supercell, creating defect–defect interactions, and thus a different system than the intent of the study. Boundary effects have been witnessed in b.c.c. supercells as large as 54 atoms, and since typical plane wave calculations scale as N^3 (where N is the number of valence electrons), the computational expense increases dramatically for larger systems. In addition, the core of the U pseudopotential is large, potentially leading to large overlap of the cores as atoms move in response to defect strain fields in certain systems. The response may be to discard pseudopotential methods in favor of more accurate techniques. However, the use of more accurate methods (FP-LMTO, etc. [18]) leads to a

limitation on system size through very high computational expense, thus limiting applicable methodologies to pseudopotential based density functional theory calculations for the investigation of defect properties.

In this work, a detailed study of defect formation in α and γ uranium using pseudopotential based DFT calculations is performed. First, the equilibrium lattice constants and the bulk modulus are calculated in both U allotropes. The vacancy formation energy in the orthorhombic α allotrope and the γ allotrope is calculated. Several systems involving self-interstitials in α-U and γ-U are investigated for the computation of interstitial formation energies. Body-centered cubic systems of U are considered with a dilute concentration of Zr in the form of substitutional and interstitial atoms, calculating the formation energies of these defects. Formation and incorporation energies of Xe, Kr, and He for various defect positions are investigated for the prediction of fission product behavior. Where mechanical instabilities occur, an approximation technique is employed to calculate defect properties.

CHAPTER 2

COMPUTATIONAL METHODS

Calculations were performed using the Vienna *ab initio* Simulation Package (VASP) [19,20,21]. The Projector-Augmented Wave method [22] is utilized within the density functional theory [23, 24] framework. Calculations are performed using the Perdew-Burke-Ernzerhof (PBE) [25] and the Perdew-Wang (PW91) [26] GGA density functional implementation for the description of the exchange-correlation. Methfessel and Paxton's smearing method [27] of the first order is used with a width of 0.2 eV to determine the partial occupancies for each wave function. Structural relaxations are performed using the conjugate gradient method until a convergence of 1 meV is reached for the total energy of the system. A uranium PAW pseudopotential with the $6s^2 6p^6 5f^3 6d^1 7s^2$ valence electronic configuration and a [Xe, 5d, 4f] core is utilized. Fission product PAW pseudopotentials (PP) used include a helium PP with the valence of $1s^2$, a xenon PP with the valence of $5s^2 5p^6$ and a [Kr, 4d10] core, and a krypton PP with the valence of $4s^2 4p^6$ and a [Ar, 3d10] core. The cutoff energy is 253 eV for the U-Xe and U-Kr systems and 479 eV for the U-He system.

The structural relaxation for the γ phase was performed on a 128 atom supercell (4x4x4) to find equilibrium lattice constants. For the α phase, a 96 atom supercell (4x2x3) was fully relaxed to calculate bulk equilibrium properties. In both systems, symmetry restrictions were removed, resulting in 36 k-points in the irreducible wedge of the Brillouin Zone (BZ). These calculations were performed for various k-point meshes, and the variance is less than 0.05 eV for a more dense mesh. Boundary effects have been observed in b.c.c. supercells as large as 54 atoms, so supercells in this study were sufficiently large to minimize cross boundary effects relating to the inherent periodicity of the system, while still remaining computationally feasible.

Defects were introduced into a supercell with equilibrium lattice constants and a structural relaxation of atomic positions was performed to calculate the formation energies. In the calculation of defect formation energies, only isolated, non-interacting defects were considered, and the energy of an isolated atom in a vacuum at its ground state is assumed to be zero, providing the reference point for the calculations [13]. The formation energy of a single vacancy is defined as

$$E_v = E_{(n-1)U} - \left[\frac{n-1}{n}\right] E_{nU} \quad (1)$$

where $E_{(n-1)U}$ is the total energy of an (n−1)U atom supercell containing one uranium vacancy, and E_{nU} is the total energy of an ideal uranium supercell containing n lattice sites. The formation energy of a U interstitial is defined as

$$E_i = E_{(n+1)U} - \left[\frac{n+1}{n}\right] E_{nU} \quad (2)$$

where $E_{(n+1)U}$ is the total energy of (n + 1)U atoms, which includes the atoms at lattice positions as well as one interstitial. The formation energy of a Zr substitutional is defined as

$$E_s = E_{(n-1)U+Zr} - \left[\frac{n-1}{n}\right] E_{nU} - E_{Zr} \quad (3)$$

where $E_{(n-1)U+Zr}$ is the energy of a lattice containing one Zr substitutional and E_{Zr} is the energy of one Zr atom in the b.c.c. allotrope. The formation energy of a Zr interstitial is defined as

$$E_i = E_{nU+Zr} - E_{nU} - E_{Zr} \quad (4)$$

where E_{nU+Zr} is the energy of a lattice containing one Zr interstitial.

The reference state for the fission gases was assumed to be an equilibrium face-centered cubic structure (f.c.c.). The f.c.c. crystal structure was chosen as the reference state due to the fact that these calculations are occurring at 0 K, and as these systems approach 0 K, they will crystallize. The ground state crystal structure for Xe and Kr is a face-centered cubic lattice. The ground state crystal structure for He is the hexagonal close-packed (hcp) lattice. However, in order to keep a consistent reference state for all incorporated external atoms, f.c.c. He is chosen as the ground state. The variance between the hcp and the f.c.c. structures for He is less than 0.01 eV. The formation energy of a single substitutional defect is defined as

$$E_s = E_{(n-1)U+FG} - \left[\frac{n-1}{n}\right] E_{nU} - E_{FG} \quad (5)$$

where $E_{(n-1)U+FG}$ is the total energy of a lattice containing one fission gas substitutional atom, E_{nU} is the total energy of an ideal uranium supercell containing n lattice sites, and E_{FG} is the energy of one fission gas atom in the face-centered cubic phase.

The formation energy of an interstitial fission gas defect is defined as

$$E_I = E_{nU+FG} - E_{nU} - E_{FG} \quad (6)$$

where E_{nU+FG} is the total energy of nU atoms and one fission gas interstitial atom. The incorporation energy of a fission gas atom is calculated according to Nerikar [28] as

$$E_{inc} = E_{nU+FG} - E_{(n+1)U} - E_{FG} \quad (7)$$

where E_{nU+FG} is the total energy of the cell with the fission product at a particular defect site, $E_{(n+1)U}$ is the total energy of the cell with a uranium atom at a particular defect site, and E_{FG} is the energy of a single fission gas atom in the reference state. The incorporation energy does not account for the formation of the defect site and assumes there is always an excess of available defect sites. A positive value of the incorporation energy means energy is required for a fission product to be placed at a particular defect site.

One issue that arises when calculating defects in U is due to the large cutoff radius of the pseudopotential used. When a defect is present and the atoms are relaxed, adjacent pseudopotential cores may overlap. A large enough core overlap can make the supercell unstable, yielding unrealistic results for the relaxed structure. Another source of anomalous structural lattice relaxation around defects is the inherent mechanical instability of the b.c.c. allotrope of U at 0 K. In order to avoid these instabilities, geometric relaxations are not performed for the whole supercell, but for a shell that consists of several full symmetric layers of nearest neighboring atoms around the defect of interest. Meanwhile, all atoms in the supercell participate in the electron density optimization. This computational strategy is illustrated in figure 1 for the interstitial in the <100> dumbbell configuration. The supercell consists of 129 atoms, all of which contribute into the electronic density optimization. The geometric optimization is performed for an inner shell of atoms with unconstrained positions that consists of two nearest neighboring layers surrounding the interstitial. The energy of the relaxed configuration $E_{(n+1)U}$ and the interstitial formation energy are connected by equation 2.

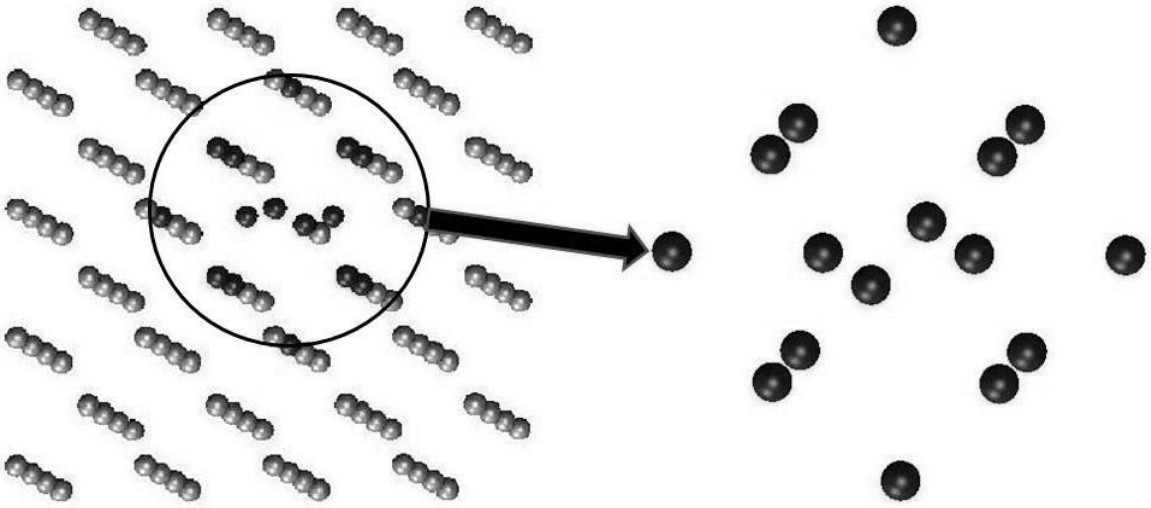

Figure 1. Schematic of the geometry used for calculating the formation energy of a <100> oriented dumbbell interstitial for a supercell with 129 atoms. Unconstrained atoms are shown as dark and constrained atoms as light. The relaxing inner shell consists of the two nearest neighbor full atomic layers surrounding the interstitial and is shown separately on the right.

This procedure is followed for all defect configurations in b.c.c. U. The choice of the shell atomic configuration for each specific defect depends on the nature of the defect as well on its symmetry. Typically, two symmetric nearest neighboring atomic layers around the defects of interest (interstitial or vacancy) were taken and these atoms were considered unconstrained during the geometric optimization. Such a procedure produces uniform, symmetrical relaxation of the defect structure and prevents any spurious reorientation of the defect caused by pseudopotential core overlap and supercell instabilities.

CHAPTER 3

BULK PROPERTIES AND INTRINSIC DEFECTS OF URANIUM

Properties of defect free γ-U

First, properties of defect free γ-U are calculated and compared with those in literature. By varying the lattice constant and calculating the energy of the system, an energy–lattice parameter curve (Birch–Murnaghan curve) [29] is generated, allowing the calculation of the equilibrium bulk modulus. The Birch–Murnaghan curve is calculated for the PW91 GGA potential and the PBE GGA potential for various k-point meshes, starting with 1× 1 × 1 and increasing sequentially to 4×4×4, in a 128 atom supercell with periodic boundary conditions for γ -U. The minimum of this curve yields the equilibrium lattice parameter and the bulk modulus is calculated from

$$B = -\frac{\partial^2 E}{\partial V^2} V \tag{8}$$

evaluated at the equilibrium lattice constant [30]. The bulk modulus was calculated with a Birch–Murnaghan curve fit for the entire total energy data (figure 2). Restricting the data set to a few points around the minimum produces changes in the bulk modulus of approximately 3%. The calculated Birch–Murnaghan curves for the PBE and PW91 functionals are shown in figures 2 and 3, respectively. Table 1 shows the lattice parameter, volume per atom, and bulk modulus calculated using both the PBE and PW91 functionals for different k-point meshes. Also shown for comparison are the values calculated by Xiang et al. [13] and Taylor [11] as well as the experimental values determined by Yoo et al. [5]. The values for the lattice parameter are within 1% of the literature values.

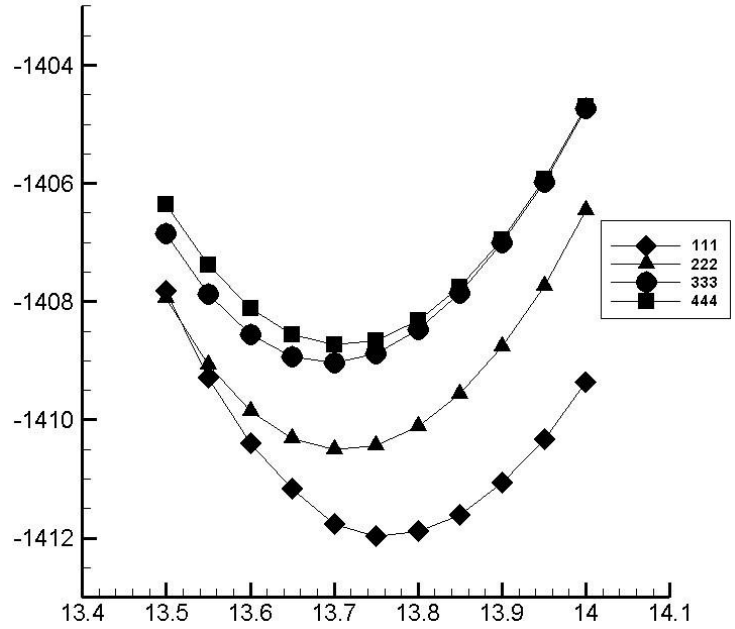

Figure 2. The total energy of the perfect b.c.c. uranium lattice as a function of the supercell lattice parameter. Calculations were performed with the PBE exchange correlation functional for different k-point meshes (1x1x1, 2x2x2, 3x3x3 and 4x4x4).

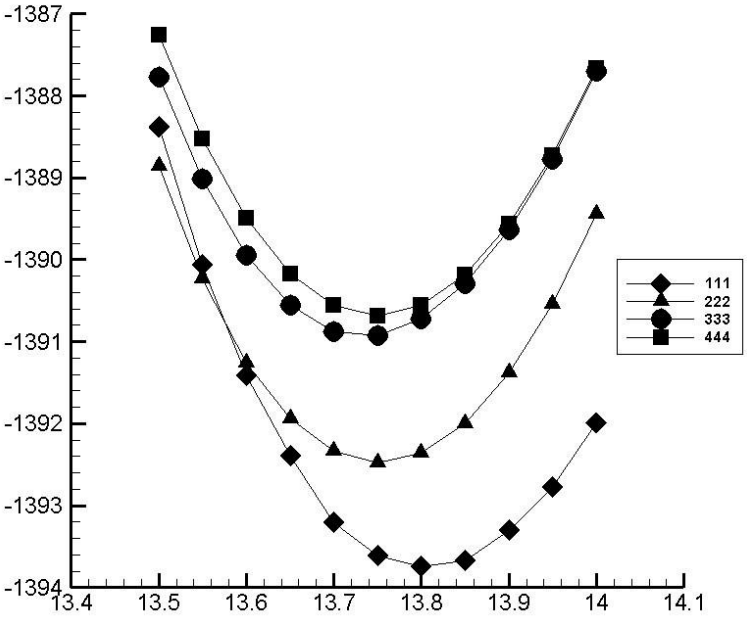

Figure 3. The total energy of the perfect b.c.c. uranium lattice as a function of the supercell lattice parameter. Calculations were performed with the PW91 exchange correlation functional for different k-point meshes (1x1x1, 2x2x2, 3x3x3 and 4x4x4).

Table 1. The properties of defect free b.c.c U: the lattice constant, volume per atom and bulk modulus. Results for both the PBE and PW91 functionals and different k-point meshes (1x1x1, 2x2x2, 3x3x3 and 4x4x4) are shown. The results are compared with the work of Xiang [13], Taylor [11] and the experimental work of Yoo [5].

		a_0 (Å)	V (Å^3)	B (GPa)
111	PBE	3.4418	20.39	138.29
	PW91	3.4525	20.58	133.41
222	PBE	3.4275	20.13	133.07
	PW91	3.4390	20.34	130.41
333	PBE	3.4235	20.06	136.29
	PW91	3.4338	20.24	133.16
444	PBE	3.4283	20.15	133.64
	PW91	3.4383	20.32	133.03
Xiang		3.4313	20.20	122.6
Taylor		3.43	20.18	176
Expt		3.419	19.98	113.3

The bulk modulus values agree better with the calculations by Xiang [13] than those by Taylor [11] and slightly overestimate the experimental value of Yoo [5]. There is a significant difference between the calculated total energies for different exchange-correlation functionals, but the values of the equilibrium lattice constant and the bulk modulus are similar for the two pseudopotentials. Increasing the density of the k-point mesh for each pseudopotential increases the total energies of the lattice, but this effect is less pronounced for finer k-point meshes. There is a general trend for the coarser k-point mesh to yield a curve that has a slightly larger lattice constant than for finer mesh grids. Likewise, the PW91 functional gives a slightly higher equilibrium lattice constant for all of the tested k-points.

Defect formation energies in γ-U

Using the equilibrium lattice parameters calculated from the analysis of defect free U, a single atom is removed from the supercell and a structural optimization is performed, where fourteen atoms (two shells) are allowed to relax. In table 2, the calculated vacancy formation energy for the PBE and PW91 functionals are compared with the experiment [17] as well as with the computational results of Xiang et al. [13].

Table 2. The formation energy of vacancies in b.c.c. U calculated using both the PBE and PW91 functionals and a k-point mesh of 4x4x4. The vacancy formation energies estimated from positron annihilation spectroscopy measurements [16] and calculated by Xiang [13] are also shown.

E^{v}_{form} (PBE)	1.384 eV
E^{v}_{form} (PW91)	1.323 eV
E^{v}_{form} (Xiang) [13]	1.08 eV
E^{v}_{form} (Matter) [16]	1.2 ± 0.25 eV

The vacancy formation energy is about 0.3 eV higher than that calculated by Xiang using a 54 atom simulation cell and PBE exchange-correlation functionals. However, results from this work are in good agreement (within the experimental error) with experiments of Matter et al. [16], who measured the positron annihilation coincidence count rate as a function of temperature and analyzed the data in terms of the trapping model, yielding relatively accurate values for the monovacancy formation energy.

For the calculation of interstitials, a single U atom is added into the supercell in different positions to calculate the formation energy from equation 2. In figure 4, the calculated interstitial formation energies for the PBE xc-functional are presented. Figure 4 also shows the atomic structure of the relaxed shell of atoms around the defect. First, it is interesting to compare the relative magnitudes of the interstitial formation energies. The formation energy of the dumbbell interstitial is heavily dependent on the orientation

of the defect, with the <111> direction having a formation energy nearly three times higher than the other two orientations. The <100> dumbbell, <110> dumbbell, and octahedral have the lowest formation energies, all below 1 eV. Thus, these configurations are predicted to be the most prevalent self-interstitials. Also noteworthy is the order of magnitude of the formation energies for interstitials. Typical formation energies for similar interstitial defects in transition metals are of the order of several electronvolt. The methodology of relaxing symmetric layered shells implemented here is not exact, and will typically overestimate the formation energy of defects, i.e., the real formation energy should be even lower. However, the fact that the formation energy of interstitials is comparable to the formation energy of vacancies is significant, since it implies similar equilibrium concentrations for these different classes of defects. The difficulty of the extraction of interstitial formation energies from experiment restricts verification of these results to previous computational work, which consists of calculations of vacancy formation energies only [14]. Of actinide metals, point defect properties of Pu have been studied. Using modified embedded-atom methods to describe interatomic interactions in plutonium, Berlu et al. [31] and Valone et al. [32] have calculated low interstitial formation energies in α- Pu. All calculated Pu self-defect dumbbell configurations and the octahedral configuration had formation energies of below 1.7 eV.

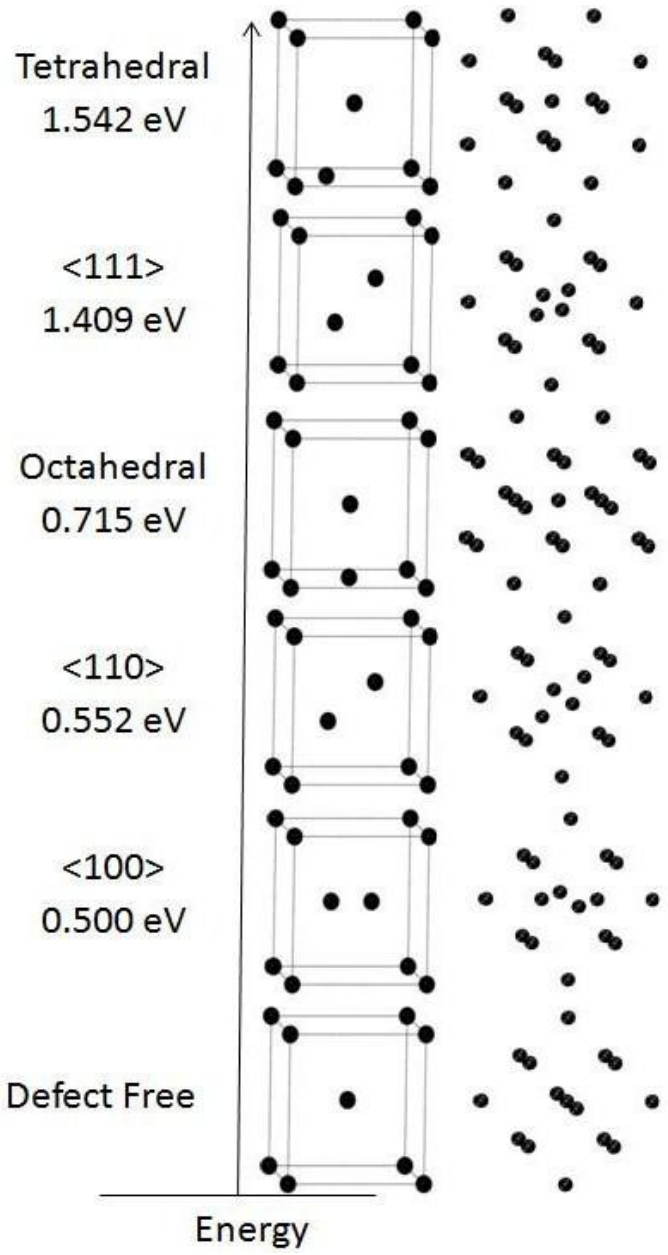

Figure 4. Self-defect formation energies calculated using the PBE exchange-correlation functional and a k-point mesh of 4x4x4. Also shown are corresponding relaxed atomic configurations for different uranium interstitials in the b.c.c. γ-U allotrope.

Defect formation energies in α-U

The face-centered orthorhombic unit cell of α-U is shown in figure 5. The α phase has a face-centered orthorhombic structure, and its conventional unit cell contains four atoms, as in face-centered cubic (f.c.c.) crystals. However, the atoms at some traditional face-centered sites are not face centers although they are on front and back faces. Further, there are no atoms on two faces of the cube; instead, one effective atom resides inside the unit cell.

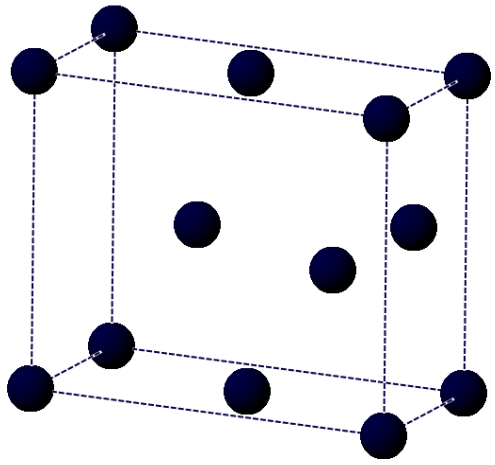

Figure 5. Schematic of the face-centered orthorhombic (A20) crystal structure of α-U.

For the analysis of α-U, a 4 × 2 × 3 supercell with 96 atoms is used. A relaxation is performed for the entire supercell, allowing the atoms themselves to relax, and also allowing the volume and shape of the supercell to change, starting with the equilibrium lattice parameters calculated by Taylor [11] and utilizing only the PBE description of the exchange-correlation functional. In table 3, the calculated equilibrium lattice parameters and volume per atom and the vacancy formation energy are compared with the results of Taylor [11]. The vacancy formation energy was also calculated to be 1.69 eV by Wirth [15].

Table 3. The lattice parameters (a, b, c and y), volume per atom and the vacancy formation energy calculated for the orthorhombic α allotrope of uranium using the PBE functional and a k-point mesh of 4x4x4. The calculated vacancy formation is compared with the results of [11].

	Taylor [13]	This Work
a (Å)	2.800	2.793
b (Å)	5.896	5.845
c (Å)	4.893	4.896
y	0.097	0.099
Volume/atom ($Å^3$)	20.19	19.98
E^v_{form} (eV)	1.95	1.86

Four interstitial structures were analyzed in the α phase of uranium: free space, and the <100>, <010> and <001> split dumbbell interstitials. The crystal structure of α-U has a relatively large open volume, placing an interstitial in this open volume is referred to as the free space defect, shown in figure 6. Split dumbbell interstitials for all three orientations are shown in figure 7.

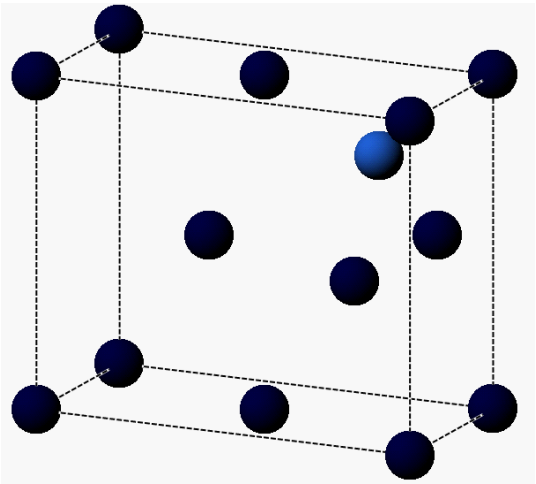

Figure 6. The free space defect in α-U. The α phase of U has a large open volume, placing a defect in the center of this open volume denotes a free space defect. Internal coordinates of the free space defect are (0.5, 0.812, 0.8) where the unit cell dimensions are (2.8, 5.896, 4.893). The free space defect is illustrated as the light blue atom.

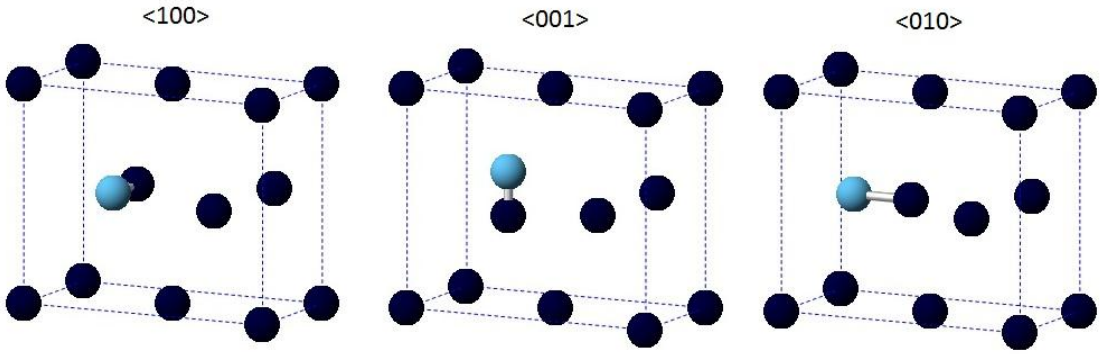

Figure 7. Schematic of split dumbbell interstitials in α-U. Three orientations of split dumbbell interstitials were analyzed: <100>, <010>, and <001>. Due to the anisotropy of the A20 structure, these three dumbbells represent very different defect configurations.

In table 4, the calculated self-interstitial formation energies in α-U are presented. The formation energies in α-U are greater than in γ-U due to α-U being a more closely-packed structure. The open volumes to incorporate defects in γ-U are larger than those in alpha. Thus, it is expected to be more difficult to create a defect in α-U, leading to higher formation energies of intrinsic and extrinsic defects. These values are slightly underestimated when compared to Wirth [15], who calculated the formation energy of the free space defect to be 4.42 eV.

Table 4. Formation energy (eV) of self-interstitials in orthorhombic α uranium for the defect configurations corresponding to those in figures 6 and 7.

	E_f
Free space	3.53
<010>	3.87
<001>	3.62

CHAPTER 4

PROPERTIES OF EXTRINSIC DEFECTS IN URANIUM

Dilute Zr defect formation energies in γ-U

Using the equilibrium lattice parameters calculated from the analysis of defect free γ-U, a single Zr atom was added into the supercell as part of a defect configuration and a structural optimization was performed. In figure 8, the calculated Zr defect formation energies for the PBE functional are presented. It is important to note that the formation energy of a substitutional defect is much lower than any configuration with an interstitial Zr atom. Thus, the substitutional position is the preferred location of dilute Zr atoms in γ-U. During irradiation, Zr may be knocked off its lattice site and occupy interstitial locations in the U–Zr lattice. These calculations show the <110> dumbbell as the lowest energy configuration for such a knocked off Zr interstitial. The tetrahedral and the <111> dumbbells are the least favorable as they have the highest formation energy.

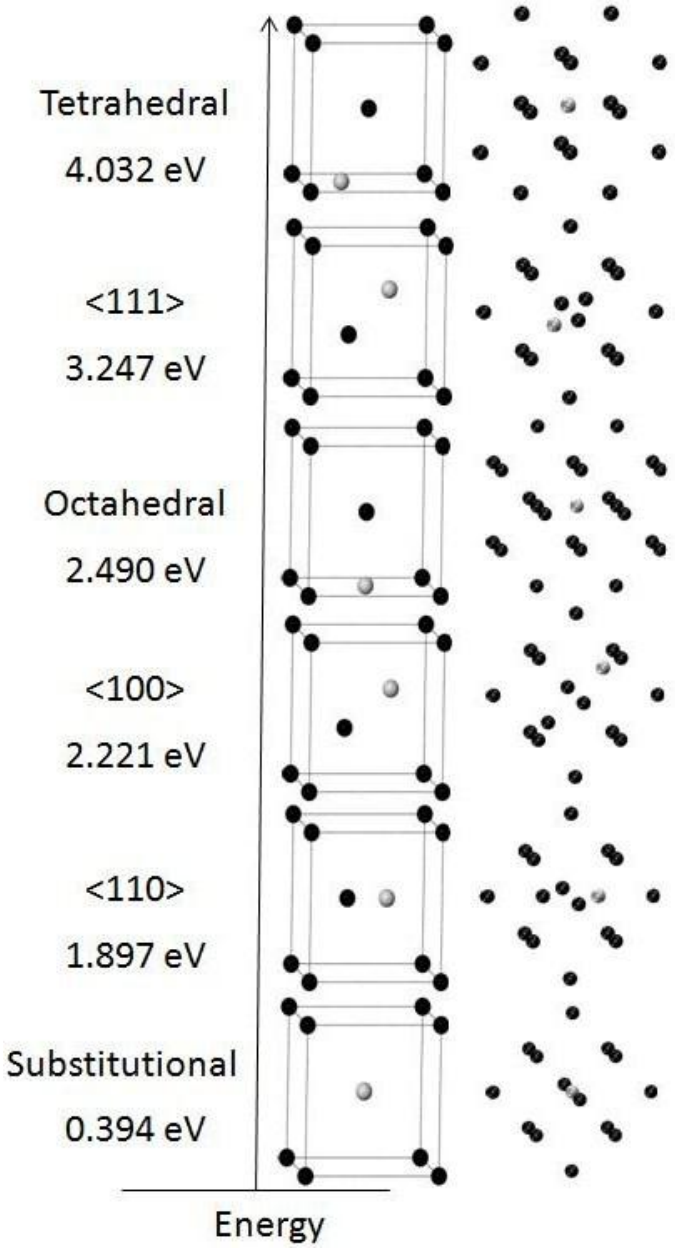

Figure 8. Zr defect formation energies calculated using the PBE functional and a k-point mesh of 4x4x4. Also shown are corresponding atomic figurations for possible Zr (white atoms) in the b.c.c. γ-U phase.

Fission Gas Defect Formation Energies and Incorporation Energies in γ-U

Using the equilibrium lattice parameters calculated from the analysis of defect free b.c.c. U, a single fission gas atom is added into the supercell to calculate the formation energy using equations 5 and 6. In table 5, the calculated substitutional and interstitial formation energies are presented and plotted graphically in figure 9.

Table 5. Formation energies (eV) of He, Xe and Kr in body-centered cubic uranium for the substitutional, <100>, <110> <111> dumbbells and the octahedral and tetrahedral interstitial positions.

	He	Xe	Kr
Sub	1.803	5.549	5.926
<100>	2.234	7.294	6.549
<110>	2.148	7.037	7.345
<111>	1.764	10.085	8.420
Octahedral	2.507	7.024	6.210
Tetrahedral	2.434	7.730	7.002

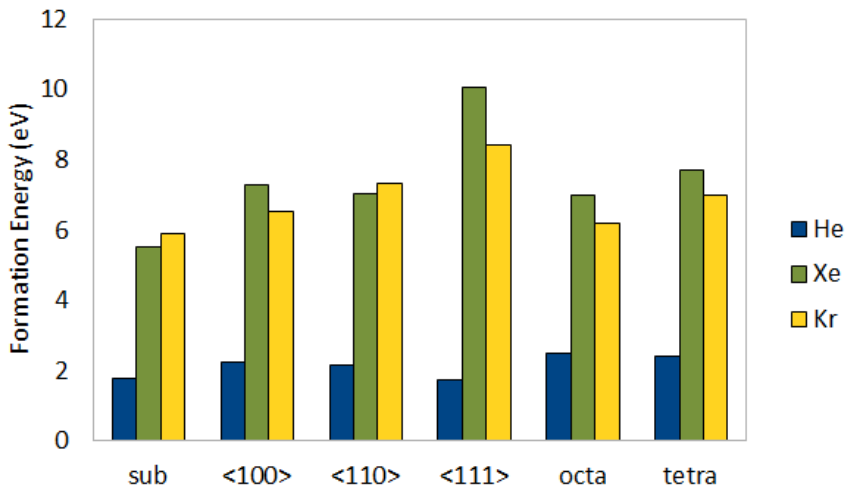

Figure 9. Formation energies (eV) of He, Xe and Kr in body-centered cubic uranium. The six positions considered are the same as the six position shown in figure 4, namely substitutional, octahedral, tetrahedral and the <100>, <110> and the <111> dumbbells.

The incorporation energies are calculated from equation 7 using uranium self-defect calculations in figure 4. In table 6, the calculated fission gas defect incorporation energies are presented and shown graphically in figure 10.

Table 6. Incorporation energies (eV) of He, Xe and Kr in body-centered cubic uranium for the same configurations as in table 5. Self-defect energies are obtained from table 4 and equation 7 is used to calculate the incorporation energies.

	He	Xe	Kr
Sub	1.803	5.549	5.926
<100>	11.312	17.752	17.007
<110>	11.279	17.548	17.855
<111>	9.986	19.686	18.020
Octahedral	11.410	17.307	16.492
Tetrahedral	10.576	17.251	16.523

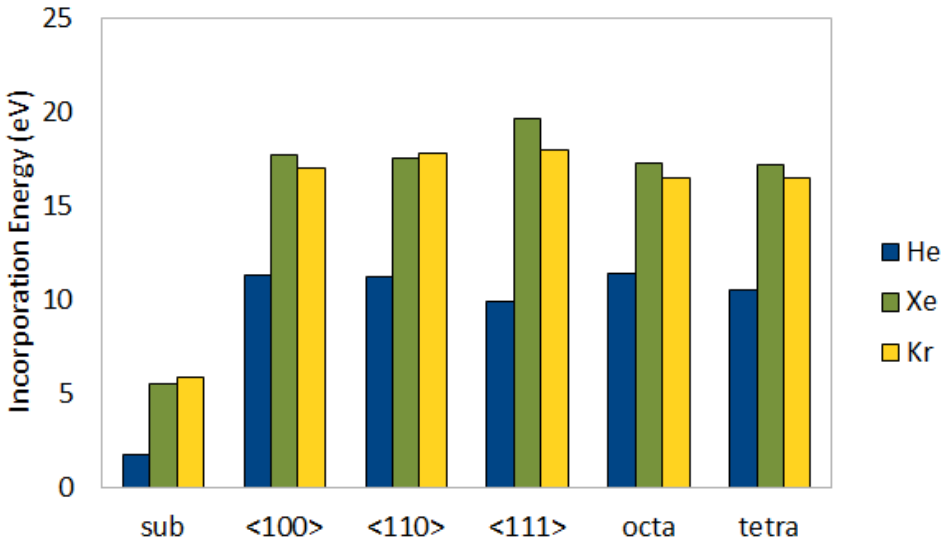

Figure 10. Incorporation energies (eV) of He, Xe and Kr in body-centered cubic uranium for the same configurations as in figure 9.

First, it is interesting to compare the relative magnitudes of the defect formation energies for each fission gas atom. There exists a general size effect with regards to the magnitude of formation energies of fission gas atoms. This is most pronounced when comparing helium with the other two atoms. Helium is a relatively small atom and thus it is expected that the defect formation energies for He are much lower than those of Xe and Kr, which are larger atoms. Also, helium formation energies in the substitutional and interstitial positions do not vary much in magnitude. In the case of the much larger Xe and Kr, it is clear that these fission products prefer to reside in the vacant lattice site rather than in an interstitial position.

This size effect is also seen in most cases while comparing Xe and Kr (Xe having the greater size), except in the case of the substitutional defect and the <110> dumbbell interstitial. This is possibly due to the very small difference between the two pseudopotential core radii, which is less than 0.11 Å (Xe core radius is 1.323 Å and Ar core radius is 1.217 Å). Also, the shell methodology is an approximation technique and there are inherent errors associated with using this technique for an energy minimization.

Valuable information can be also gleaned by analyzing the relative magnitudes of the different defect configurations. There is a total variance of approximately 0.75 eV from the most energetically favorable defect configuration to the most energetically unfavorable configuration for He. Thus, it is expected that He will be found in a variety of defect positions in b.c.c. U. For Xe and Kr, the formation energy of the defect is heavily dependent on the orientation, with the <111> dumbbell having the highest formation energy and the substitutional site the lowest for both elements. Thus, the <111> dumbbell configuration is predicted to be the least prevalent defect type and the substitutional the most prevalent. It makes physical sense that a substitutional defect would have the lowest formation energy, as a vacant uranium lattice position has a much greater volume than any other defect site. Thus, the overall localized deformation will be minimized by Xe or Kr inhabiting a vacancy. The formation energy of all fission gas

defects in γ-U is larger than self-defects. The maximum self-defect formation energy has been calculated to be approximately 1.5 eV (figure 4), whereas the minimum He defect formation energy is 1.76 eV. Thus, it is more energetically favorable for b.c.c. U to form a self-defect, than to form a fission gas defect. The shell methodology employed will typically overestimate the formation energy of defects, i.e., the formation energy should be lower than the values presented here.

The octahedral-tetrahedral migration mechanism seems appropriate for fission gases based on the energies of these respective defect configurations. Energy differences between these two configurations are below 0.8 eV for all fission product species. Given that an octahedral or tetrahedral defect is present, fission product diffusion is likely to occur via this mechanism. The difficulty of the extraction of interstitial formation energies from experiment and the lack of previous computational work on fission gas defects in metallic uranium means there is no comparison for benchmarking these values. On the basis of these results, it is expected that Xe and Kr would occupy vacant U lattice sites rather than interstitial positions. Also, it is apparent that helium may be found in either substitutional or interstitial positions with the difference in energies of these configurations being much smaller. While no calculations of the migration energy were performed, it is apparent that helium would be a more mobile species, with transitions from interstitial to substitutional and vice versa resulting in less energy differences. It would be expected that Xe and Kr would migrate by a substitutional vacancy exchange mechanism, with relatively high values of the migration barrier for such an exchange. Given the computational complexity, it is not yet possible to perform calculations of the migration pathway using DFT methods.

Fission Gas Defect Formation Energies and Incorporation Energies in α-U

In table 7, the calculated substitutional and interstitial formation energies for defects in α-U are presented and shown in figure 11. In order to calculate incorporation energies of fission gas defects in α-U, self-defect formation energies of defects in α-U are needed. Self-defect formation energies are given in table 4.

Table 7. Formation energies (eV) of He, Xe and Kr in orthorhombic uranium for the substitutional, free space defect and the <010> and <001> dumbbell configurations.

	He	Xe	Kr
Sub	3.33	6.13	6.03
Free space	3.63	12.25	10.26
<010>	3.82	11.58	10.17
<001>	3.65	10.65	9.63

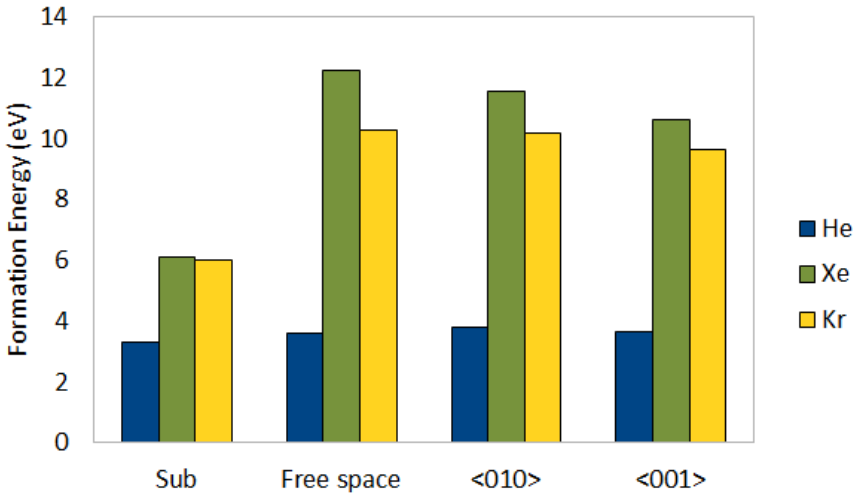

Figure 11. Formation energies (eV) of He, Xe and Kr in orthorhombic uranium in the substitutional, free space defect and <100>, <010> and <001> configurations. These correspond to the configurations shown in figures 6 and 7 (substitutional is not shown).

Using the self-defect energies from table 4, the incorporation energies were computed and are presented in table 8 and figure 12.

Table 8. Incorporation energies (eV) of He, Xe and Kr in orthorhombic uranium obtained from equation 7 using data in tables 7 and 4.

	He	Xe	Kr
Sub	3.33	6.13	6.03
Free space	9.62	20.00	18.00
<010>	9.47	18.98	17.57
<001>	9.55	18.31	17.29

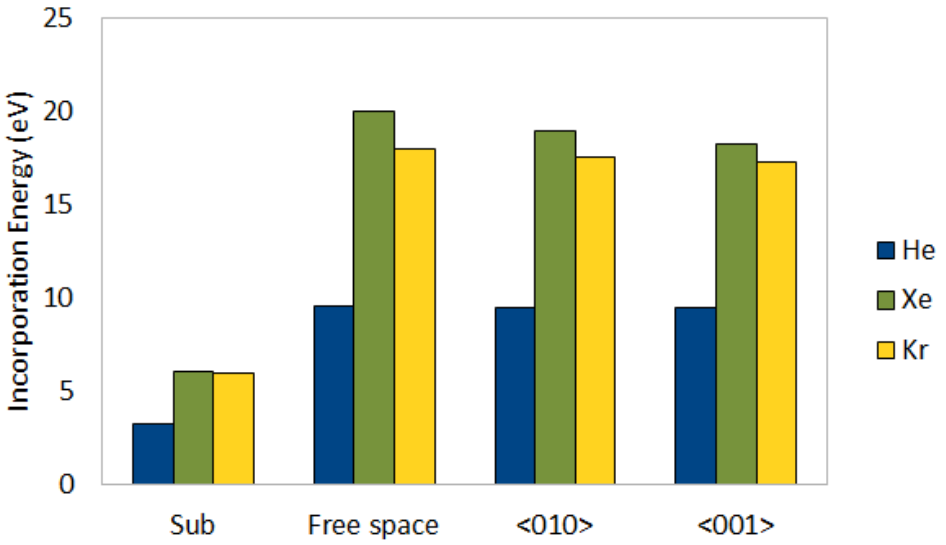

Figure 12. Incorporation energies (eV) of He, Xe and Kr in orthorhombic uranium for the configuration as described in figures 6, 7, and 11.

In α-U, similar trends are observed to those in γ-U for extrinsic gas defects. Helium exhibits the lowest formation energy of fission product species analyzed, with a variance of less than 0.5 eV between defect positions. Size effects appear to dominate formation energies for the α phase. Xenon is the largest fission product species analyzed and has the highest formation energies, while He is the smallest species investigated and

has the lowest formation energies. For Xe and Kr, the substitutional site is the preferred defect location. It is interesting to note that formation energies of fission products in α-U are generally higher than those in γ-U. This results from α-U having a more closely-packed crystal structure than the γ phase. The octahedral and tetrahedral volumes in γ-U are larger than the free space defect volume in α-U. Also, α-U is a more rigid structure in terms of elastic constants, so it is expected that the formation of dumbbell interstitials would be more difficult than in γ-U. In comparing the formation energies of fission gases to the self-defects, the Xe and Kr defects are less energetically favorable, but He formation energies are comparable.

The fuel undergoes phase transformations during initial operation as well as when it is cooled down. In addition, during operation, temperatures at the fuel pin periphery suggest that the alpha phase is present. Thus, the fact that formation energies of gas atoms are higher in the alpha U structure implies that the phase transformation from gamma to alpha may affect the fission gas behavior in the fuel. Higher formation energies imply higher strain fields associated with the defect incorporation leading to stress concentrators and incipient crack nucleation sites during reactor cool down and also during operation.

Comparisons can be made to a previous computational study of fission products in UO_2 [26]. A DFT based analysis of Xe in UO_2 yielded an incorporation energy of 11.11 eV for Xe interstitials. The work presented here has found that Xe interstitial incorporation energies in pure metallic U range from 17-20 eV, significantly higher than that for UO_2. The fluorite structure of UO_2 has a large open volume and thus can more readily include fission product defects. Thus, higher incorporation energies for pure metallic U are expected.

CHAPTER 5

CONCLUSIONS

Previously, there has been a limited amount of research into the calculation of fundamental properties of metallic uranium, particularly related to point defects. In this work DFT calculations are performed using VASP with PAW pseudopotentials. Several important bulk material properties for γ-U are reproduced that agree well with other published results. Calculation of the formation energy for a vacancy was performed in the γ and α allotropes of U. The vacancy formation energy in the α allotrope compares very well with previously published computational work. The vacancy formation energy in the γ allotrope agrees well with previously published computational and experimental work. Formation energies for various interstitial configurations were also calculated, for which there is no experimental data or other calculations to serve as a benchmark. The most likely positions for self-interstitial U atoms in γ-U are the <110> dumbbell, <100> dumbbell, and octahedral interstitials. Self-interstitial atoms are likely to be found in a variety of configurations in α-U. The first comprehensive study for dilute Zr defects in the b.c.c. allotrope of U shows that the substitutional defect is expected to be the prevalent occupation site. The formation energies have been calculated for He, Xe, and Kr in various defect configurations in the α and γ phases, for which there is no experimental or computational data to serve as a benchmark. The most likely position for dilute Xe and Kr atoms in γ-U is the substitutional site. Dilute He atoms in γ-U are likely to be found in a wide variety of defect positions due to the comparable formation energies of all defect configurations analyzed. In α-U, He atoms are likely to be found in several different defect locations, while Kr and Xe are likely to be found as substitutionals. In both the α and γ phases, size effects of fission products appear to dominate, as smaller fission product species generally have lower formation energies.

REFERENCES

[1] G. Hofman, L. Walter and T. Bauer, *Prog. Nucl. Energy* **31** (1997) 83

[2] W. Carmack, D. Porter, Y. Chang, S. Hayes, M. Meyer, D. Burkes, C. Lee, T. Mizuno, F. Delage and J. Somers, *J. Nucl. Mater.* **392** (2009) 139

[3] Basic Research Needs For Advanced Nuclear Energy Systems, Report of the Basic Energy Sciences Workshop on Basic Research Needs for Advanced Nuclear Energy Systems, 2006.

[4] D.R. Olander, Fundamental Aspects of Nuclear Reactor Elements, NTIS, ERDA, 1975.

[5] C. Yoo, H. Cynn and P. Söderlind, *Phys. Rev. B* **57** (1998) 10359

[6] P. Söderlind, *Adv. Phys.* 47 (1998) 959

[7] Hofman, Hayes, Petri, *J. Nucl. Mater.* **227** (1996) 277

[8] P. Söderlind, *Phys. Rev. B* **66** (2002) 085113

[9] C. Barrett, M. Mueller and R. Hitterman, *Phys. Rev.* **129** (1963) 625

[10] J. Crocombette, F. Jollet, L. Nga and T. Petit, *Phys. Rev. B* **64** (2001) 104107

[11] C. Taylor, *Phys. Rev. B* **77** (2008) 094119

[12] G. Kresse and J. Furthmüller, *Phys. Rev. B* **54** (1996) 11169

[13] S. Xiang, H. Huang and L. Hsiung, *J. Nucl. Mater.* **375** (2008) 113

[14] H. Matter, J. Winter and W. Triftshäuser, *J. Nucl. Mater.* **66** (1979) 085113

[15] G.-Y. Huang and B. Wirth, *J. Phys: Condens. Matt.* **23** (2011) 205402

[16] J. Sanchez and D. de Fontaine, *Phys. Rev. Lett.* **35** (1975) 227

[17] Y. Ye, Y. Chen, K. Ho and B. Harmon, *Phys. Rev. Lett.* **58** (1987) 1769

[18] D. Price and B. Cooper, *Phys. Rev. B* **39** (1989) 4945

[19] G. Kresse, J. Furthmuller, *Phys. Rev. B* **54** (1996) 11169

[20] G. Kresse, D. Joubert, *Phys. Rev. B* **59** (1999) 1758

[21] P. Blochl, *Phys. Rev. B* **50** (1994) 17953

[22] P. Blochl, O. Jepsen, O. Anderson, *Phys. Rev. B* **49** (1994) 16223

[23] P. Hohenberg, W. Kohn, *Phys. Rev.* **136** (1964) B864

[24] W. Kohn, L. Sham, *Phys. Rev.* **140** (1965) A1133

[25] J. Perdew, K. Burke, M. Ernzerhof, *Phys. Rev. Lett.* **77** (1996) 3865

[26] J. Perdew, Y. Wang, *Phys. Rev. B* **45** (1992) 13244

[27] M. Methfessel, A. Paxton, *Phys. Rev. B* **40** (1989) 3616

[28] P. Nerikar, X-Y. Liu, B. Uberuaga, C. Stanek, S. Phillpot, S. Sinnott, *J. Phys.:Condens. Matter* **21** (2009) 435602

[29] F. Birch, *Phys. Rev.* **71** (1847) 809

[30] M. Cohen, *Phys. Rev. B* **32** (1985) 7988

[31] L. Berlu, G. Jomard, G. Rosa and P. Faure, *J. Nucl. Mater.* **372** (2008) 171

[32] S. Valone, M. Baskes, M. Stan, T. Mitchell, A. Lawson and K. Sickafus, *J. Nucl. Mater*. **324** (2004) 41